C Journal of Carbon Research

MDPI

Article

Charcoal in Anaerobic Digestion: Part 1—Characterisation of Charcoal

Hans Korte [1], Jan Sprafke [1,*], Pooja Girdharbhai Parmar [2], Thomas Steiner [2], Ruth Freitag [2] and Volker Haag [3]

[1] Department of Waste and Resource Management, Faculty of Agricultural and Environmental Sciences, University of Rostock, 18059 Rostock, Germany
[2] Department for Process Biotechnology, Faculty of Engineering Sciences, University of Bayreuth, 95447 Bayreuth, Germany
[3] Thuenen Institute of Wood Research, 21031 Hamburg, Germany
* Correspondence: jan.sprafke@uni-rostock.de

Abstract: Biochar (BC) is often used as an additive in anaerobic digestion (AD) to increase yield and/or to stabilise the process when the manure content is increased. Unfortunately, BC is rarely described in detail in terms of its raw material sources, production processes, and structural, physical and chemical properties to allow correlation with its effects on AD. It is an open question whether microorganisms from AD can penetrate into different biochar pore types, depending on their wood origin. In this paper, we describe the preparation (temperatures, treatment times, yields) and characterisation shrinkage, density, pore sizes, pore size distribution, specific surface area, ash, volatiles, fixed carbon, elemental composition, polycyclic aromatic hydrocarbons (PAHs), polychlorinated biphenyls (PCBs), benzene, toluene, ethyl-toluene, xylene (BTEX) and volatile halogenated hydrocarbons (VHH) of BC cubes of Scots pine (*Pinus sylvestris*) and common beech (*Fagus sylvatica*) powder made from this BC in addition to commercial charcoal powder. The pore size distribution determined by mercury porosimetry differs from that determined by 3D-reflected light microscopy. After incubating BC cubes in AD, the cubes were mechanically cleaned and cut into two pieces. Microorganisms were detected inside the cubes by fluorescence microscopy. Particle size and wood source determine the influence of BC on AD.

Keywords: biochar (BC); pine; beech; anaerobic digestion (AD); microorganisms; fluorescence microscopy; three-dimensional-reflected light microscopy; porosimetry; specific surface; elemental composition

Citation: Korte, H.; Sprafke, J.; Parmar, P.G.; Steiner, T.; Freitag, R.; Haag, V. Charcoal in Anaerobic Digestion: Part 1—Characterisation of Charcoal. *C* **2024**, *10*, 77. https://doi.org/10.3390/c10030077

Academic Editor: Dimitrios Kalderis

Received: 28 May 2024
Revised: 1 August 2024
Accepted: 7 August 2024
Published: 26 August 2024

1. Introduction

Anaerobic digestion (AD) is an established process for the production of biogas from various types of biomass such as municipal waste (organic waste, sewage sludge), industrial and commercial residues, agricultural biomass (e.g., maize, sugar beet, straw, manure, etc.) or residues from landscape management. In Germany, there are currently around 8700 biogas production plants in operation [1]. Some of them upgrade biogas by separating biomethane (CH_4) from carbon dioxide (CO_2) and other minor components. In addition, most biogas plants produce and transmit electricity and thermal energy through combined heat and power (CHP) modules in energy grids. In the past, government support (Renewable Energy Sources Act) guaranteed fixed prices for electricity fed into the grid over a 20-year period. Due to the newly started revaluation of CO_2 in terms of global warming potential (GWP_{100}) and monetary reimbursement for CO_2 saved or avoided, some biogas plants are now restructuring and changing to liquefy biomethane and CO_2 to sell to the market and stopping power generation, the funding for which is ceasing in the near future.

The agricultural sector in Germany "produces" about 209 million metric tonnes of manure per year [2], of which about one-quarter to a third is already used for biogas. Potentially, another third could also be used economically. This would be achieved with existing plant capacity. In practice, large plants with an electrical capacity of more

than 1000 kW often consume more than 30,000 t/a of biomass. Depending on substrate availability, process inhibition, economic aspects and legal framework, the manure concentration has to be optimised. In these large plants, the average manure concentration is less than 30%. Increasing manure concentration leads to an increase in protein and its degradation products, ammonia (NH_3) and ammonium (NH_4^+), that inhibit the microbial community in AD [3].

It has long been known from the literature that the use of BC is suitable for increasing biogas yield in AD [4] although with increased levels of inhibitors such as NH_3 and NH_4^+ [5].

In a critical review, Kumar et al. [6] list six properties of BC (porosity, specific surface area, cation exchange capacity, electrical conductivity, surface functional groups, redox properties) that are thought to influence AD. Tang S. et al. [7] add particle size, elements and pH value to this list. Of course, particle size and porosity are elemental structures of BC in contact with microorganisms in AD. It has been reported that microorganisms can live within the BC particles [8,9]. Unfortunately, the article by Heitkamp et al. [8] only characterises BC as "Carboferm", a wood-based capillary BC, without any further details, e.g., type of wood, particle size, or other physical or chemical analytical data. Lü et al. [9] characterise their BC as obtained by the pyrolysis of fruit wood (without further specification). In many publications concerning the use of BC in AD [4,8,9], the origin of the pyrolysis feedstock, e.g., bamboo or eucalyptus, instead of botanical names is insufficiently described. The same applies to the production methods, e.g., process equipment, temperature/time regime and/or product characteristics.

The type of BC feedstock such as bamboo, straw, husks, wood, etc., plays an important structural role. For example, a typical European conifer, such as Scots pine (*Pinus sylvestris*) studied in this paper, consists of about 93% (area per cent of a specimen for light microscopy) of tracheids, cells of approximately 3100 µm length and approximately 45 µm width (including the cell walls). The tracheids are axially oriented and connected tangentially in radial walls by elliptical pits of several micrometres high that can be closed by tori [10,11]. The maintenance or structural change in tori and pits in BC depends on the severity of the pyrolysis.

Common beech (*Fagus sylvatica*), a typical European hardwood consisting of several cell types, including relatively short (300–700 µm) vessel elements in the longitudinal direction, which are joined into tubes and have a diameter of 30–100 µm, accounting for about 29%, and fibres with a length of about 1200 µm and a lumen diameter of about 5 µm, accounting for about 40% in the tissue [10]. The wood structure is largely retained during pyrolysis, but in a reduced form due to shrinkage. The BC structure can be used to identify the wood species the BC was made from. Haag et al. [12] have shown that sometimes the wood species of commercial charcoal does not match the information on the packaging.

Our aim is to increase the manure content in AD to more than 50% and to stabilise the process by adding charcoal. The effect on fermentation and viscosity will be published as "Charcoal in anaerobic digestion: Part 2—Influence of charcoal on anaerobic digestion" elsewhere.

This paper deals with the production and characterisation of BC cubes of approximately $6 \times 6 \times 6$ mm^3 and rods made from Scots pine (*P. sylvestris*) and common beech (*F. sylvatica*) produced simultaneously in a 90-litre batch retort [13] and will be compared with commercial charcoal powder (CCP). By comparing the structural characteristics of the BC types with the characteristics of the AD microorganisms, we clarify what might be living in the charcoal and have a look into the opened cubes to see if microorganisms are colonising them. BC is characterised chemically by its wood resources and processing conditions, according to the European Biochar Certificate (EBC) [14]; structurally by microscopy; and physically by surface area, specific surface area, pore size and pore volume distribution.

2. Materials and Methods

The uncharred beech and pine wood samples were analysed by classic light microscopy. Transverse and radial sections (approximately 25 µm thick) were sequentially cut from

solid heartwood samples using a sliding microtome and stained with a solution of safranin and astra blue to study microstructural details. The study was carried out using a digitised image analysis system (analySIS®, Olympus, Tokyo, Japan) mounted on an Olympus AX 70 microscope. To characterise the charred samples, a 3D-reflected light microscopy technique (digital microscope VHX-5000, Keyence, Neu-Isenburg, Germany) was used to visualise the characteristic structural features [15]. Transverse and tangential section measurements were performed on three samples of pine and beech. Quantitative characteristics were measured on the average of at least 50 measurements of each parameter studied [16]. The average tangential tracheid diameter in pine was only measured in the first third of the earlywood tracheids, which can be clearly distinguished from the narrow latewood. The average pit diameter (vertical) was measured to characterise the volume change in the axial direction.

Softwood, Scots pine (*P. sylvestris*) and hardwood, common beech (*F. sylvatica*) were pyrolysed as cubes with starting dimensions of 8 × 8 × 7 mm^3 or rods of 8 × 8 × 500 mm^3 in a 90 L retort, a closed cylindrical vessel with a lid and a central degassing tube with an opening at the bottom (Figure 1). Cubes were used as they are and rods were ground to powder for use in AD and chemical characterisation. The temperature was recorded close to the bottom and close to the lid near the inner wall of the retort. The retort was heated with a 10.5 kW gas stove using a 5.5 kg (netto) propane gas container. Once a sufficient temperature was reached in the retort, heating was assisted by combustible outgassing wood gases. The retort contained 4 baskets, placed approximately 2.5 cm above the bottom of the retort to pyrolyse cubes and rods of two types of wood simultaneously in this project. The bottom of the retort contained 12 × 3 holes of 4 mm in diameter in the radial direction which were closed with screws resulting in a reducing atmosphere in the retort (Pyr_{red}). To increase the functional groups at the surface of the charcoal, the holes in the bottom were open for pyrolysis. The hot retort was then removed from the oven and placed on a tray filled with sand. Water was then applied to the sand and the steam generated by the hot retort was channelled through the bottom holes in the retort, partially oxidising the charcoal (Pyr_{ox}), and was discharged through the central tube.

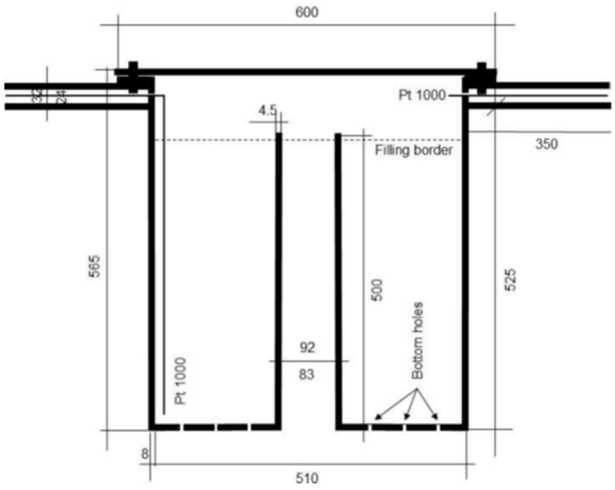

Figure 1. Ninety-litre retort with central degassing tube and bottom holes for steam treatment.

Temperature was measured with Pt 1000 elements and data were recorded with a Voltkraft data logger DL-240K (Conrad Electronic, Wernberg-Köblitz, Germany). Dimensions of wood and BC cubes were measured with callipers. BC rods were ground using a Retsch cutting mill SM 2000 and a Retsch ZM 1000 centrifugal mill. Chemical analysis according to EBC [14] was performed externally (Wessling GmbH, Hannover, Germany), as well as pore size according to ISO 15901-1 [17], density according to DIN 66137 [18] and specific surface area analysis according to DIN ISO 9277 [19] (3P Instruments GmbH, Odelzhausen, Germany). CCP was purchased as Nerolit 10 µm from PHK Polymertechnik

GmbH, Wismar, Germany, a charcoal powder with particle size d90 of less than 10 µm, a fineness that we cannot produce on our laboratory equipment.

Microorganisms in biochar cubes were observed by using the LIVE/DEAD BacLight Bacterial Viability Kit (Catalogue number L7012, Invitrogen, Waltham, MA, USA) under a fluorescence microscope (Olympus BX51, Olympus, Tokyo, Japan) to monitor the viability of bacteria and archaea by examining the integrity of the cell membrane. Cells with damaged membranes which are considered dead or dying, are stained red, while cells with intact membranes are stained green. BC cubes were collected from the anaerobic digesters and frozen. BC samples were cleaned at the surface with a scalpel, cut and scraped from the centre on glass slides under sterile conditions. Samples were stained with the dye mixture and incubated for 15 min in the dark at room temperature prior to analysis. The following excitation/emission maxima were used to detect the fluorescence of the dyes: 480/500 nm for SYTO9 and 490/635 nm for propidium iodide (PI). All images were analysed using the computer program analySIS (Soft Imaging System, Münster, Germany).

The functional groups of BC were analysed using the universal attenuated total reflectance–Fourier transform infrared spectroscopy (UATR−FTIR) accessory, used with a Spectrum Two FTIR spectrometer (Perkin Elmer Inc., Waltham, MA, USA). Samples were prepared by crushing biochar cubes in a mortar and pestle. Powdered samples were directly placed on the top of the diamond-covered platform and pellets were manually pressed until the "force gauge" was at 100. Spectra were recorded in 4000–600 cm^{-1} wave number range using the Spectrum IR computer program.

3. Results and Discussion

One hundred cubes of pine and beech were callipered, weighed, placed in a wire basket and placed among the other cubes of the same type in the retort baskets. After closing the retort and the furnace, the fire was started by igniting the propane gas stove. The pyrolysis process was completed after approximately 1200 min (20 h) when the gas filling of the vessel was complete. A typical temperature versus time curve is shown in Figure 2. The maximum temperature of 541 °C measured near the lid near the cylinder wall was reached after 200 min, corresponding to a heating rate of 2.7 °C min^{-1}. After 125 min, 275 °C was reached, the temperature at which the autogenous exothermic charring reaction starts [20]. The combustible wood supports the gas cooker as it leaves the retort through the central tube. Pyrolysis is complete after about 340 min, when the temperature reaches about 250 °C; the temperature that can be reached in the specific furnace with the propane stove alone.

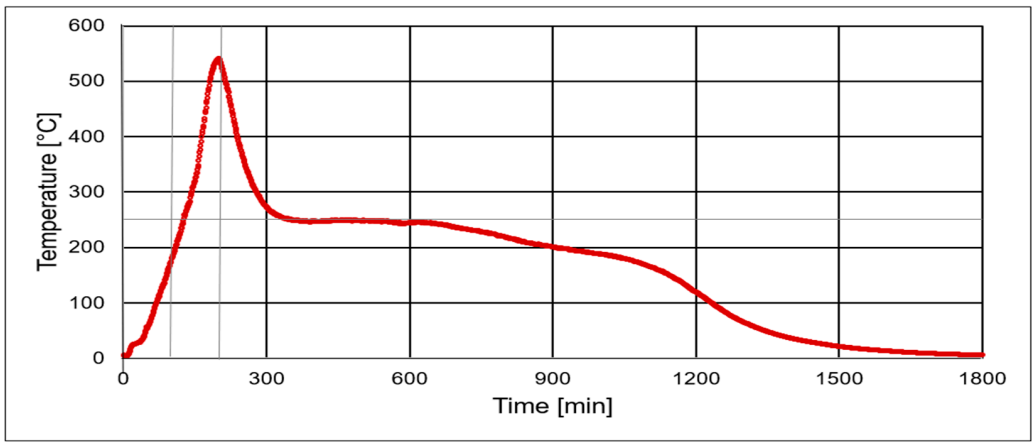

Figure 2. Typical temperature vs. time curve of a pyrolysis process in reducing atmosphere with Scots pine and common beach cubes and rods placed in 4 baskets. Heating with a 5.5 kg propane gas bin until the gas bin was empty.

After opening the retort, the pyrolysed pine and beech cubes were removed from the wire baskets, callipered and reweighed. The average dimensions and weights of 100 wood and charcoal cubes are given in Table 1.

Table 1. Average dimensions and weights of 100 cubes of Scots pine (*Pinus sylvestris*) and common beech (*Fagus sylvatica*) before and after pyrolysis. Calculated are density, yield, volume shrinkage and carbonisation factor. BC = biochar, sdv = standard deviation, Vol. = volume, shrink. = shrinkage.

	Weight [g]	sdv [%]	Vol. [cm^3]	sdv [%]	Density [g cm^{-3}]	sdv [%]	Yield [%] (*w*/*w*)	Vol. Shrink. to [%]	Carbonisation Factor
Beech wood	0.341	7.7	0.477	5.0	0.715	6.2			
Beech BC	0.093	11.2	0.209	10.2	0.445	9.6	27%	44%	3.7
Pine wood	0.237	17.0	0.459	9.4	0.516	14.8			
Pine BC	0.069	13.8	0.197	12.7	0.350	13.8	29%	43%	3.4

The (envelope) density decreased from 0.72 g cm^{-3} to 0.45 g cm^{-3} (loss of 36.6%) for beech and from 0.52 g cm^{-3} to 0.35 g cm^{-3} for pine (loss of 32.7%). The volume shrank to 44% for beech and 43% for pine, corresponding to an average linear shrinkage in one dimension of about 75%. Charcoal yield by weight was 27% for beech and 29% for pine, figures known from the literature [20] corresponding to the carbonisation factors (1/yield) of 3.7 for beech and 3.4 for pine.

An impression of the wood and BC cubes is given in Figure 3. It can be seen that the structure remains in place but at a reduced size. There are no visible cracks in the BC cubes. Wide and narrow annual rings are easily visible in pine wood and BC (white arrows in Figure 3).

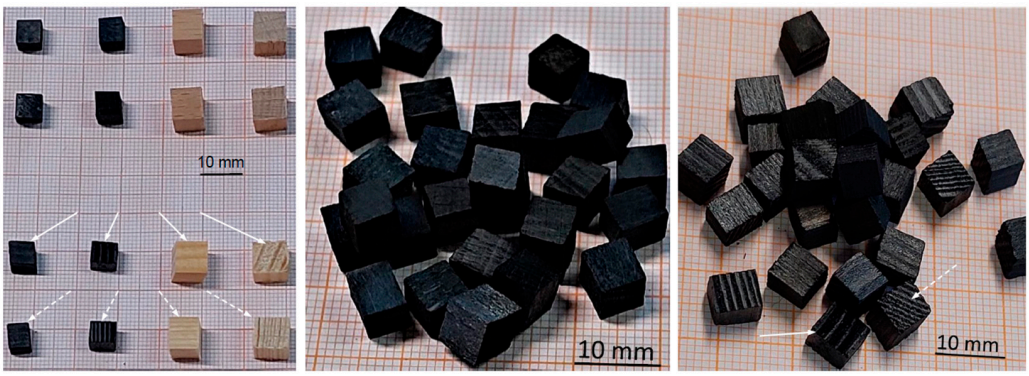

Figure 3. Wood (common beech and Scots pine) and charcoal cubes. **Left**: upper side beech, lower side pine. Solid lines: wide growth rings; dashed lines: narrow growth rings. **Middle**: beech charcoal, **right**: pine charcoal, solid lines: wide growth rings; dashed lines: narrow growth rings.

We compare two different types of pyrolysis. One with closed holes in the bottom of the retort, resulting in an overall reduced atmosphere (Pyr_{red}) (Figure 2), and a second with open holes for a partially oxidising atmosphere and final steam treatment (Pyr_{ox}).

Pyr_{ox} differed from Pyr_{red} in that way, that a second thermometer was placed near the cylinder wall close to the bottom between two baskets. The temperature versus time curves are shown in Figure 4. The two temperature curves are very different in height.

Near the bottom, the temperature rose to over 400 °C within 60 min, but only reached 130 °C near the lid. For both Pt 1000 elements, it is important to note that their tips measure the surrounding gaseous atmosphere (at room temperature both Pt elements showed the same temperature comparable to other thermometers). We therefore have no information about the temperatures inside the wood/coal itself. Both temperature curves show that the exothermic reaction started after about 160 min, reaching about 740 °C near

the bottom and about 480 °C near the lid after about 190 min. This experimental set-up shows that temperature data given in the literature must be treated with caution unless the experimental set-up is not described and the location of the temperature sensor is indicated.

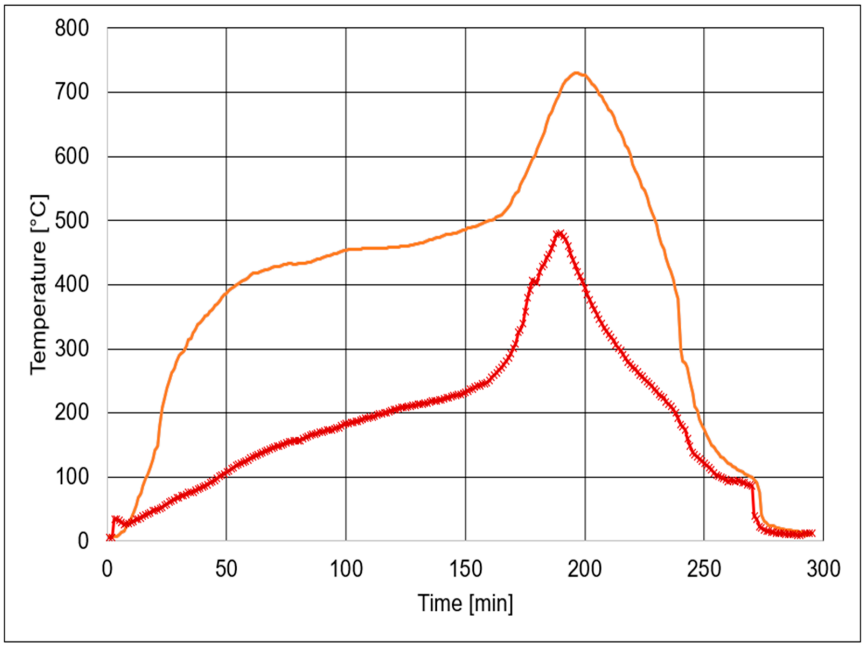

Figure 4. Temperature vs. time curves of pyrolysis with final partial oxidation conditions. Thermometer placed close to the bottom (upper orange line) and thermometer placed close to the lid (lower red line with crosses). After 220 min, the retort was flooded with steam.

The furnace was opened after 180 min but still was burning. The retort was removed after 220 min and placed on a tray filled with sand. Water was immediately added to the sand and steam passed through the retort, exiting through the central tube and a central tube in the tray. Three minutes later the cylinder was further cooled by spraying the retort with a watering can. After 270 min, the lid was unscrewed, the retort opened and the baskets removed. BC cubes and rods were also basted to avoid burning.

Pine and beech BC rods were ground to powder for chemical analysis. The results are given in Table 2. Fixed carbon was very high with 93.3% ± 0.6% for all four samples. EBC defines BC with organic carbon between 35% and 95% [14]. Total volatile carbons, therefore, are low. The molar ratios of hydrogen to carbon are between 0.20 and about 0.25 for the self-made charcoal and 0.10 for the CCP. They therefore meet the EBCs highest quality requirement of less than 0.40. No EBC values are given for the molar ratio of oxygen to carbon. Pine BC from Pyr_{red} has a ratio of 0.0248 and 0.0282 for Pyr_{ox}, which is an increase of about 14% due to the steam treatment. For CCP, the ratio is 0.0354. The O/C ratio gives an indication of the amount of oxygen-containing side groups. The levels of chlorine, bromine, fluorine and sulphur are also very low.

Table 2. Sum parameter, elemental analysis and analytics from calorimetric digestion of charcoal powder made from Scots pine, common beech rods and CCP. Pyr_{red} with sealed retort bottom holes and Pyr_{ox} with open holes and final steam treatment.

	Unit	Pine Rods Pyr_{red}	Pine Rods Pyr_{ox}	Beech Rods Pyr_{ox}	CCP
Sum parameter					
Water content	%(w/w)	0.65	1.1	3.25	6.3
Ash (815 °C)	%(w/w)	1.45	1.05	1.6	3.5
Volatiles	%(w/w)	4.70	5.50	5.43	3.78
Fixed carbon	%(w/w)	93.9	93.45	93	92.75

Table 2. *Cont.*

	Unit	Pine Rods Pyr_{red}	Pine Rods Pyr_{ox}	Beech Rods Pyr_{ox}	CCP
Elemental analytics					
Carbon	%(*w*/*w*)	94.65	94.4	94.1	94.55
Hydrogen	%(*w*/*w*)	2	1.85	1.6	0.83
Nitrogen	%(*w*/*w*)	0.22	0.19	0.23	0.155
$Oxygen_{calc.}$	%(*w*/*w*)	3.13	3.56	4.07	4.464
$H/C_{calc.}$	mol/mol	0.254	0.236	0.204	0.105
$O/C_{calc.}$	mol/mol	0.0248	0.0282	0.0324	0.0354
Analytics from calorimetric digestion					
Chlorine, total	%(*w*/*w*)	0.013	0.0155	0.016	0.03
Sulphur, total	%(*w*/*w*)	0.03	0.03	0.035	0.035
Bromine, total	%(*w*/*w*)	<0.008	<0.008	<0.008	<0.009
Fluorine, total	%(*w*/*w*)	<0.008	<0.008	<0.008	<0.009

With the exception of chromium and nickel, all the elements analysed in Table 3 are at low levels and below the EBC limits. We do not have a clear indication of the source of the high levels of chromium and nickel, but we assume that they are from the steel material of the retort.

Table 3. Elements from aqua regia digestion of charcoal powder made from Scots pine and common beech rods and commercial coal powder CCP. Pyr_{red} with sealed retort bottom holes (Figure 2) and Pyr_{ox} with open holes and final steam treatment (Figure 4). EBC comparison values for quality levels EBC-Feed/EBC-Feed Plus.

	Unit	Pine Rods Pyr_{red}	Pine Rods Pyr_{ox}	Beech Rods Pyr_{ox}	CCP	EBC
Elements from aqua regia digestion						
Aluminium (Al)	%(*w*/*w*)	<0.0003	0.001	<0.0003	0.032	
Arsenic (As)	mg/kg	<1.0	<1.0	<1.0	<1.1	2
Beryllium (Be)	mg/kg	0.00	<0.00	0.01	<0.00	
Calcium (Ca)	%(*w*/*w*)	0.25	0.23	0.35	0.99	
Cadmium (Cd)	mg/kg	<0.03	<0.03	<0.03	0.63	0.8
Cobalt (Co)	mg/kg	2.1	2.6	2.7	0.23	
Chromium (Cr)	mg/kg	135	126	122	4.3	70
Copper (Cu)	mg/kg	5.9	5.3	6.1	10	70
Iron (Fe)	%(*w*/*w*)	0.058	0.057	0.055	0.038	
Potassium (K)	%(*w*/*w*)	0.24	0.11	0.46	0.61	
Sodium (Na)	%(*w*/*w*)	0.002	0.013	0.012	0.047	
Nickel (Ni)	mg/kg	77	73	71	1.7	25
Phosphorus (P)	%(*w*/*w*)	0.016	0.016	0.019	0.099	
Lead (Pb)	mg/kg	<0.30	<0.30	<0.31	0.97	10
Antimony (Sb)	mg/kg	<2.0	<2.0	<2.1	<2.1	
Selenium (Se)	mg/kg	<2.0	<2.0	<2.1	<2.1	
Silicon (Si)	%(*w*/*w*)	0.002	0.037	0.004	0.041	
Tin (Sn)	mg/kg	<1.0	<1.0	<1.0	<1.1	
Tellurium (Te)	mg/kg	<5.0	<5.1	<5.2	<5.3	
Titanium (Ti)	%(*w*/*w*)	0.024	0.056	0.056	0.001	
Vanadium (V)	mg/kg	0.34	0.29	0.31	0.16	
Zinc (Zn)	mg/kg	5.2	7.7	5.5	91	200
Mercury (Hg)	mg/kg	<0.10	<0.10	<0.10	<0.11	0.1

Polychlorinated biphenyls (PCBs) as given in Table 4 are below the detection limit in all four samples. The situation is different for polycyclic aromatic hydrocarbons (PAH)

from toluene extraction in Table 4. Self-generated BC are below the detection limit for all PAHs, but CCP, except for acenaphthylene, show detectable concentrations of a total of 916 mg kg^{-1}. This is high, compared to EBC which sets the level at 6 + 2.4 mg kg^{-1}.

This low level in the EBC is a precautionary measure.

> *"In absence of investigations how PAHs in biochar may pose risks to the environment and health, it was easier and faster to use the lowest known limit values for any type of soil amendment and apply it for biochar"* [14].

Table 4. Polychlorinated biphenyl (PCB) and polycyclic aromatic hydrocarbons (PAH) of charcoal powder made from Scots pine, common beech rods and CCP. Pyrolysis in reducing atmosphere (Pyr_{red}) and pyrolysis with final oxidation step (Pyr_{ox}).

	Unit	Pine Rods Pyr_{red}	Pine Rods Pyr_{ox}	Beech Rods Pyr_{ox}	CCP
PCB (polychlorinated biphenyl)					
PCB Nr. 28	mg/kg	<0.1	<0.1	<0.1	<0.1
PCB Nr. 52	mg/kg	<0.1	<0.1	<0.1	<0.1
PCB Nr. 101	mg/kg	<0.1	<0.1	<0.1	<0.1
PCB Nr. 138	mg/kg	<0.1	<0.1	<0.1	<0.1
PCB Nr. 153	mg/kg	<0.1	<0.1	<0.1	<0.1
PCB Nr. 180	mg/kg	<0.1	<0.1	<0.1	<0.1
Sum of 6 PCB	mg/kg	-/-	-/-	-/-	-/-
PCB total (Sum 6 PCB x 5)	mg/kg	-/-	-/-	-/-	-/-
PCB Nr. 118	mg/kg	<0.1	<0.1	<0.1	<0.1
Sum of 7 PCB	mg/kg	-/-	-/-	-/-	-/-
PAH (polycyclic aromatic hydrocarbon)					
Naphthalene	mg/kg	<1	<1	<1	9.18
Acenaphthylene	mg/kg	<1	<1	<1	<1
Acenaphthene	mg/kg	<1	<1	<1	4.91
Fluorene	mg/kg	<1	<1	<1	6.83
Phenanthrene	mg/kg	<1	<1	<1	69.4
Anthracene	mg/kg	<1	<1	<1	21.3
Fluoranthene	mg/kg	<1	<1	<1	156
Pyrene	mg/kg	<1	<1	<1	108
Benzo(a)anthracene	mg/kg	<1	<1	<1	66.2
Chrysene	mg/kg	<1	<1	<1	112
Benzo(b)fluoranthene	mg/kg	<1	<1	<1	110
Benzo(k)fluoranthene	mg/kg	<1	<1	<1	47.0
Benzo(a)pyrene	mg/kg	<1	<1	<1	100
Dibenz(a,h)anthracene	mg/kg	<1	<1	<1	9.71
Benzo(ghi)perylene	mg/kg	<1	<1	<1	52.3
Indeno(1,2,3-cd)pyrene	mg/kg	<1	<1	<1	43.8
Sum of detected PAHs	mg/kg	-/-	-/-	-/-	916

EBC does not give figures for concentrations of benzene, toluene, ethylbenzene and xylene (BTEX) or volatile halogenated hydrocarbons (VHH). VHH were below or close to detection limits for all four BC samples (Table 5). BTEX concentrations were low for self-made BC but high for CCP. The highest concentration of 2400 mg kg^{-1} was found for

benzene and 410 mg kg^{-1} for toluene. In total, BTEX amounted to 2810 mg kg^{-1}. Obviously, these figures are critical for feed applications, but will be tested for poisoning in AD.

Table 5. Benzene, toluene, ethylbenzene and xylene (BTEX) and volatile halogenated hydrocarbons (VHH) of BC powder made from Scots pine, common beech rods and CCP. Pyrolysis in reducing atmosphere (Pyr_{red}) and pyrolysis with final oxidation step (Pyr_{ox}).

	Unit	Pine Rods Pyr_{red}	Pine Rods Pyr_{ox}	Beech Rods Pyr_{ox}	CCP
BTEX (benzene, toluene, ethylbenzene, xylene)					
Benzene	mg/kg	3.8	<0.5	0.5	2400
Toluene	mg/kg	0.8	0.5	0.5	410
Ethylbenzene	mg/kg	<0.2	<0.2	<0.2	4.1
m-, p-Xylene	mg/kg	<0.2	<0.2	<0.2	20
o-Xylene	mg/kg	<0.2	<0.2	<0.2	3.9
Sum of BTEX	mg/kg	4.6	0.5	1	2.800
VHH (volatile halogenated hydrocarbons)					
Dichlormethane	mg/kg	<2	<2	<2	<2
cis-1,2-Dichlorethene	mg/kg	<0.2	<0.2	<0.2	<0.2
Trichlormethane	mg/kg	<0.2	<0.2	<0.2	<0.2
1,1,1-Trichlorethane	mg/kg	<0.1	<0.1	<0.1	<0.1
Tetrachlormethane	mg/kg	<0.2	<0.2	<0.2	0.3
Trichlorethene	mg/kg	<0.1	<0.1	<0.1	<0.1
Tetrachlorethene	mg/kg	<0.1	0.5	<0.1	0.2
Sum of VHH	mg/kg	-/-	0.5	-/-	0.5

In summary, the results of the analysis show that there is little chemical difference between self-made charcoal, regardless of the type of wood, the duration of pyrolysis and/or reducing or oxidising atmosphere.

The charcoal powder was also analysed by UATR−FTIR spectroscopy for functional group characterisation/identification (Figure 5).

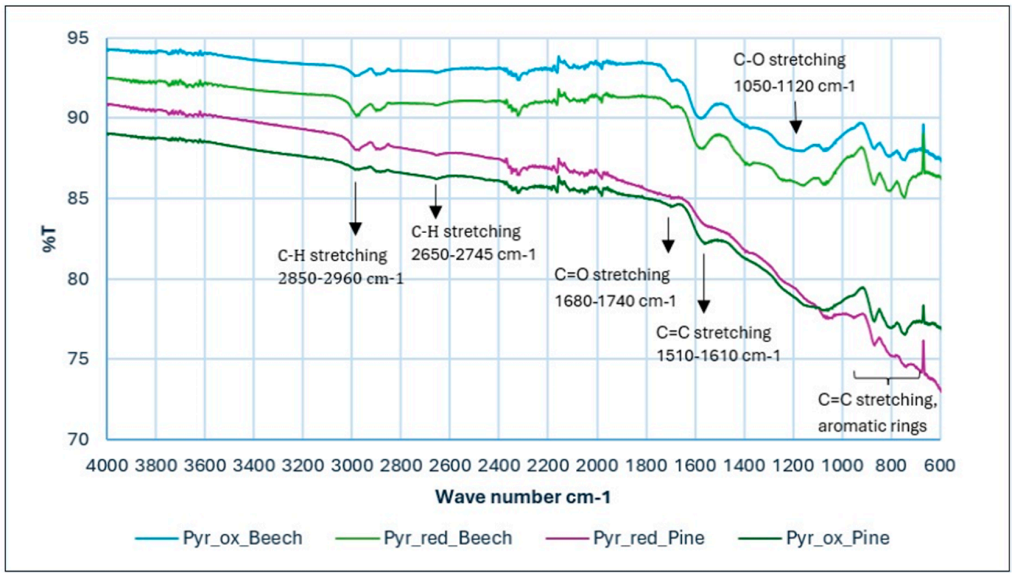

Figure 5. UATR−FTIR spectra of beech and pine biochar samples from pyrolysis in reducing (Pyr_{red}) or oxidising atmosphere (Pyr_{ox}).

In Figure 5, the graph shows the IR spectra of both types of wood treated with the two pyrolysis methods. Particularly the functional groups are marked as described in the literature. The detected peak found in the region of wave number 2650–2745 cm^{-1} for the C-H stretching vibration indicates the presence of aldehyde, together with another possible peak appearing in the region of wave number 1680–1700 cm^{-1}, indicating C=O stretching in the ketone and aldehyde [21]. The peak in the region of 1610–1510 cm^{-1} wave number belongs to C=C stretching [22–24]. The broad peak appeared in the region of 1155–1200 cm^{-1} for the C-O stretching bond in cellulose and hemicellulose [22]. The peak region of 1000–600 cm^{-1} is the fingerprint region; peaks appearing in this region are for the aromatic ring, formed due to the C=C bond stretching in the alkene at the higher temperature biochar [25].

The IR spectra obtained shows how the functional groups present in the biochar showed similarity with respect to different wood species. The spectra do not allow quantification of functional groups. There was no obvious difference between the Pyr_{ox} and Pyr_{red} spectra of beech BC. For the pine BC, the only difference was found at C=C stretching at 1660–1740 cm^{-1} but this bonding does not belong to an oxidising step.

To study the pore structure of the BC samples, we used mercury (Hg) intrusion porosimetry. In Hg intrusion porosimetry, the sample pores are intruded by mercury with increasing pressure, filling first the large pores and then the smaller ones. The curves in Figures 6 and 7 show the pore size distribution of wood and BC on a logarithmic scale, starting on the left-hand side with large pores. For better interpretation of the pore size distribution, derivation curves are shown in dotted lines as well.

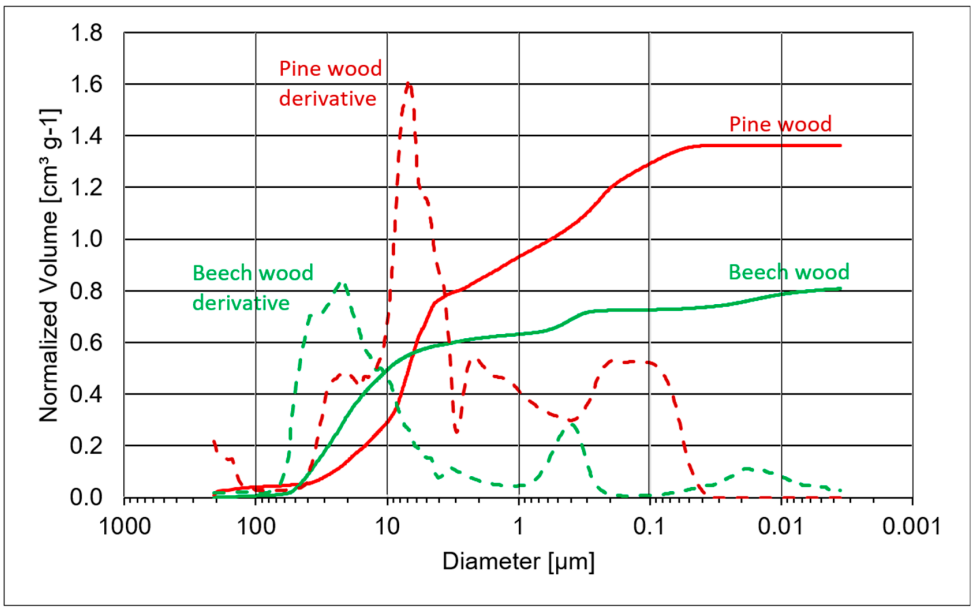

Figure 6. Pore size distribution of common beech (green solid) and Scots pine (red solid) measured with mercury porosimetry. Derivation curves as dotted lines in the corresponding colours. Big pores on the left, small ones on the right.

The filling of beech wood pores starts at about 70 µm and ends at about 4 nm (Figure 6). There are two peaks in the derivative curve of beech for large pores at about 40 µm and about 23 µm and one for small pores at about 4 µm. The results for large pores differ to the values given in the literature and our own findings (see Figure 8A,B and Table 6). Wagenführ [10] reported tangential vessel diameters of 30 ⋯ 100 µm and a frequency of 80 ⋯ 130 ⋯ 160 vessels mm^2. Therefore, we conclude that Hg intrusion porosimetry seems to underestimate large vessels. The small pores of about 4 µm correspond to pore diameters of fibres (see Figure 8A).

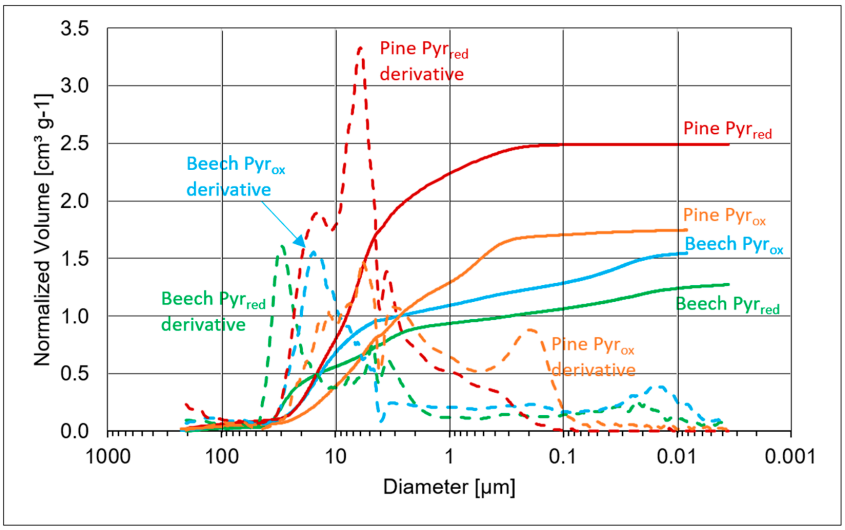

Figure 7. Pore size distribution of pine BC Pyr_{red} (red solid), pine BC Pyr_{ox} (orange solid), beech BC Pyr_{ox} (blue solid) and beech BC Pyr_{red} (green solid) measured with mercury porosimetry. Derivation curves as dotted lines in the corresponding colours. Big pores on the left, small ones on the right.

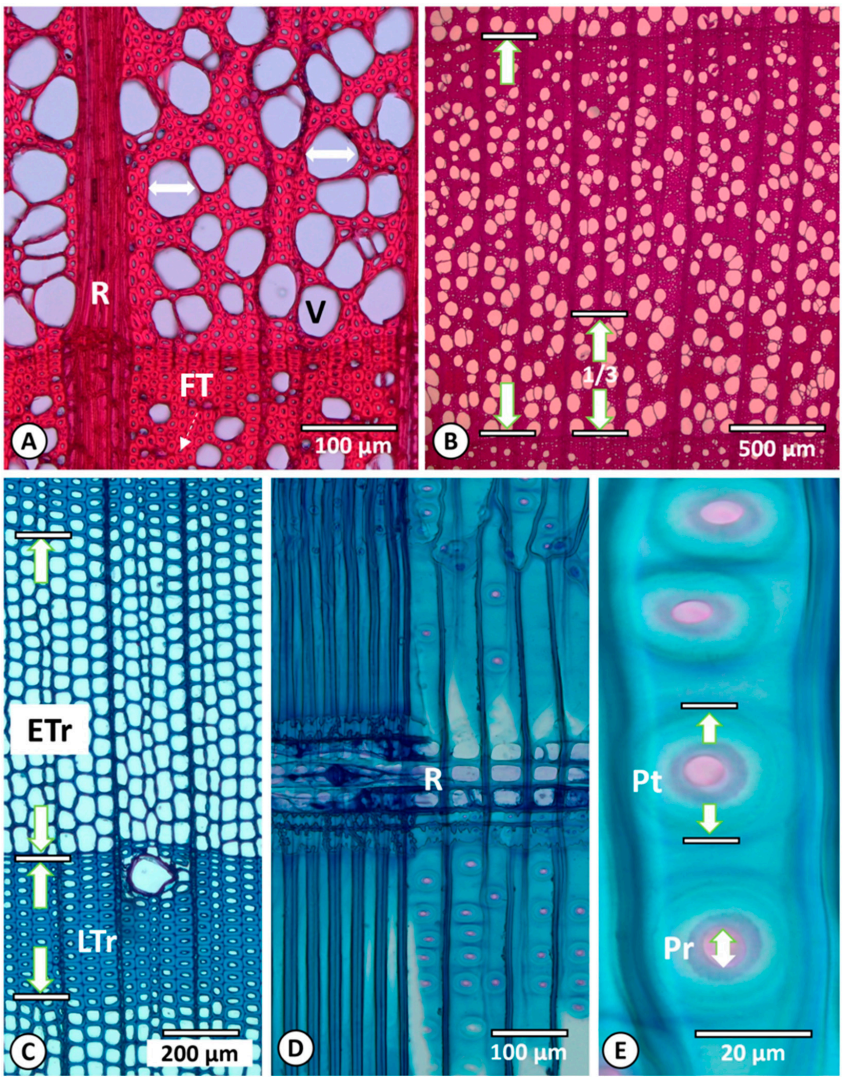

Figure 8. Classic light microscopy of (**A**) *Fagus sylvatica*: transverse section with vessels (V), tangential vessel diameter (solid white arrows), rays (R) and fibre tracheids (FT) with small pores (dotted white

arrow); (**B**) *F. sylvatica*: transverse section with schematic representation of the measuring range in the front third of a growth ring (arrows on the left, a complete growth ring and on the right a third in comparison); (**C**) *Pinus sylvestris*: transverse section with schematic illustration of areas with early wood tracheids (ETr) and late wood tracheids (LTr); (**D**) *P. sylvestris*: radial section with ray (R) and characteristic window-like pinoid crossfield pits; (**E**) *P. sylvestris*: radial section showing the measurements of the average pit size (Pt) and pit aperture size (Pr), both measured vertically.

Table 6. Diameters of beech vessels and pine tracheids in tangential direction and pit diameter in axial direction.

Beech Tangential Vessel Diameter	**Wood**			**Mdv**	**Charcoal**			**Mdv**
Cube identity	BW1	BW2	BW3		BC1	BC2	BC3	
Minimum value	61.1	48.2	55.2	48.2	28.8	35.1	24.6	24.6
Middle value	85.2	72.1	71.8	76.3	53.4	54.8	41.6	49.8
Maximum value	110.6	94.7	94.1	110.6	74.1	69.3	57.6	74.1
Standard deviation	9.1	9.0	7.2	10.5	9.2	7.6	6.0	9.7
Pine tangential tracheid diameter								
Cube identity	PW1	PW2	PW3		PC1	PC2	PC3	
Minimum value	14.1	21.1	14.1	14.1	14.7	12.8	12	12
Middle value	33.4	38.0	32.8	34.7	25.0	21.1	20.9	22.4
Maximum value	49.4	53.1	51.7	53.1	34.4	36	30.2	36
Standard deviation	7.7	6.2	7.4	7.5	4.2	3.8	3.7	4.4
Pine axial pit diameter								
Cube identity	PW1	PW2	PW3		PC1	PC2	PC3	
Minimum value	15.9	17.0	17.7	15.9	12.5	13.2	13.7	12.5
Middle value	21.3	22.7	22.5	22.3	17.5	17.0	17.3	17.2
Maximum value	24.7	27.0	28.2	28.2	23.1	20.9	20.8	23.1
Standard deviation	1.7	2.3	2.2	2.2	1.9	1.6	1.6	1.7

For pine wood, the filling of large pores starts at about 40 µm and ends at about 0.18 µm. The pore volume of pine wood is about 70% higher than that of beech wood. The pore diameters of large pores show a peak in the derivation curve at about 25 µm which is in good accordance with our own findings (see Figure 8E and Table 6) and the literature [10] with tangential tracheid diameters of about 40 µm of early wood tracheids. Late wood tracheids have much thicker cell walls resulting in smaller pore diameters. Therefore, the "average" diameter of 25 µm is a good result. The peak of the small pores with a derivation curve peak at about 8 µm corresponds to pit apertures in tracheids.

"Downward peaks" at about 3–4 µm are artefacts due to the change in the pressure regime.

The pore-size distribution curves of beech and pine BC of Pyr_{red} and Pyr_{ox} are shown in Figure 7. Compared to the pore size distribution of wood (Figure 6), pine BC shows higher amounts of pores than beech BC, but there are also large differences between Pyr_{red} and Pyr_{ox}.

The pore sizes and distribution in beech BC differs between Pyr_{red} and Pyr_{ox}. In Pyr_{red}, large pores start at around 45 µm and end at around 10 µm with a peak at around 30 µm followed by a second pore cluster with a peak at about 5 µm and a third long stretched small cluster from about 1 µm to 6 nm. Beech BC from Pyr_{ox} shows large pores from about 40 µm to about 5 µm with a peak at about 15 µm and small pores from about 100 nm to 10 nm. Pine BC Pyr_{red} and Pyr_{ox} also differ. Large pores of Pyr_{red} start at about 35 µm and show a shoulder peak at about 15 µm followed by a second major peak at about 6 µm. The smallest pores end at about 0.1 µm. Large pores of pine BC from Pyr_{ox} start at about 33 µm, with a shoulder peak at about 15 µm followed by a higher peak also at

about 6 µm. There is also a second cluster of pores from about 1 µm to about 0.2 µm. Steam treatment in Pyr_{ox} resulted in the appearance of or increase in small pores in pine BC and very small pores in beech BC.

An overview of skeletal density (density without pores), specific surface area (SSA), specific pore volume (SPV), modal value of pore size distribution (PS Mod), median value of pore size distribution (PS Med) and porosity, which is the ratio of pore volume to total volume of wood before and after pyrolysis treatment is given in Table 7.

Table 7. Skeletal density, specific surface area (SSA), specific pore volume (SPV), pore size distribution modal value (PS Mod), pore size distribution median value (PS Med) and porosity of beech and pine wood and BC cubes.

	Density [g cm^{-3}]	SSA [m^2 g^{-1}]	SPV [cm^3 g^{-1}]	PS Mod [µm]	PS Med [µm]	Porosity [%]
Beech wood cubes	1.385	0.21	0.720	21.8	17.1	49.9
Pine wood cubes	1.269	0.26	1.320	7.6	5.5	62.6
Beech BC cubes Pyr_{red}	1.493	267	1.237	29.6	6.0	64.9
Pine BC cubes Pyr_{red}	1.395	237	2.400	6.1	6.3	77.0
Beech BC cubes Pyr_{ox}	1.415	201	1.518	15.5	7.1	68.2
Pine BC cubes Pyr_{ox}	1.483	279	1.719	5.8	3.3	71.8

The skeletal density is determined with helium (He) pycnometry. Beech wood cubes, at 1285 g cm^{-3}, are slightly denser than pine wood cubes, at 1.269 g cm^{-3}. Both values are lower than in the literature where the skeletal density of wood is given as 1.45 g cm^{-3} to 1.5 g cm^{-3} [20]. After pyrolysis, the skeletal density only increases a little by 0.1 g cm^{-3} for beech BC and about 0.2 g cm^{-3} for pine BC. CCP has a skeletal density of 1.635 g cm^{-3}.

According to Brewer [26], the skeletal density correlates with the pyrolysis temperature. Densities of close to 1.5 g cm^{-3} are achieved with mesquite biochar at about 480 °C. In our pyrolysis experiments, we certainly reached higher temperatures of more than 700 °C (Figure 4), but corresponding high skeletal densities were not found.

In contrast to the skeletal densities, there were very large differences in the SSA of wood and BC. Both woods are below 0.3 m^2 g^{-1}, with pine wood (0.26 m^2 g^{-1}) being slightly higher than beech wood (0.21 m^2 g^{-1}). Pyrolysis increased the SSA to more than 200 m^2 g^{-1}. In Pyr_{red}, beech BC shows a higher SSA with 267 m^2 g^{-1} compared to pine with 237 m^2 g^{-1}. In Pyr_{ox}, it is the other way round with 201 m^2 g^{-1} for beech and 279 m^2 g^{-1} for pine BC. CCP has an SSA of 418 m^2 g^{-1}.

Specific pore volume (SPV) is the number used to quantify the pore volume in cubic centimetres per gram (cm^3 g^{-1}) of sample. Pine wood cubes with an SPV of 1.32 cm^3 g^{-1} showed more than 80% more pore volume than beech wood cubes with an SPV of 0.72 cm^3 g^{-1}. Beech BC cubes from Pyr_{red} showed an increase of 72% compared to wood and pine BC cubes of 81%. The SPV of beech Pyr_{ox} was more than double that of wood and 22% higher than that of Pyr_{red}. For pine BC cubes, the results were vice versa. The Pyr_{red} of pine was about 40% higher in SPV than Pyr_{ox}. Although the pore diameters decreased (Figures 6 and 7), the SPV increased. The reason is the decrease in density (Table 1). It is evident that SSA does not correlate with SPV.

The modal value of the pore size distribution corresponds to the maximum of the pore size distribution curves, which can be found as peaks in the derivative curves of Figures 6 and 7. It corresponds to the visual impression that the largest pores of beech wood and BC are larger than those of pine wood and BC. Due to shrinkage (Table 1), the pores of BC are smaller than wood pores, except for beech BC Pyr_{red}, which has pore diameters of 29.6 µm compared to 21.8 µm for beech wood.

The median value of the pore size distribution corresponds to the median d_{50} value of the particle size distribution, with 50% of the pores being smaller and 50% larger than the median value. Beech wood cubes with a median of 17.1 µm show that there are fewer

smaller pores compared to pine wood and all BC which look very similar at a level of 3.3 to 7.1 µm.

The total volume of wood or BC samples is made up of the volume of the solid components and the pore volume. The pore volume of pine wood at 62.6% is 25% higher than that of beech wood at 49.9%. Porosity increased by pyrolysis from 49.9% for beech wood to 64.9% and 68.2% for beech BC Pyr_{red} and Pyr_{ox}. Pine BC also showed an increased porosity of 77.0% and 71.8% for Pyr_{red} and Pyr_{ox} compared to pine wood at 62.6%.

Wood and BC cubes were also analysed by classical optical microscopy and 3D-reflected light microscopy. Figure 8 shows cross sections of beech wood (A and B) and pine (C). The radial section is shown in Figure 8D, with details of the pits shown in E. Beech showed large vessels surrounded by small fibres and parenchyma cells. In contrast, pine showed relatively homogeneous tracheid cells that differed mainly in wall thickness and radial extent in early wood (ETr) and late wood (LTr). Pit size and pit aperture size can be clearly distinguished (D). In contrast to the microscopic determination of solid wood samples, charcoal cannot be prepared as flat (planar) slices because the wood tissue is strongly decomposed by pyrolysis and becomes very brittle. In 3D-reflected light microscopy, the uneven surfaces are digitally scanned. The first step is to create three-dimensional images, which then are converted into two-dimensional images. The terminology for and description of the wood structure is based on the IAWA lists of microscopic characteristics for hardwood identification [27] and also for softwood identification [28]. To minimise the variation in the results, vessel diameters were only measured in the first third of a growth ring (Figure 8B). In order to estimate axial shrinkage, pine pit aperture sizes were measured (Figures 8E and 9C).

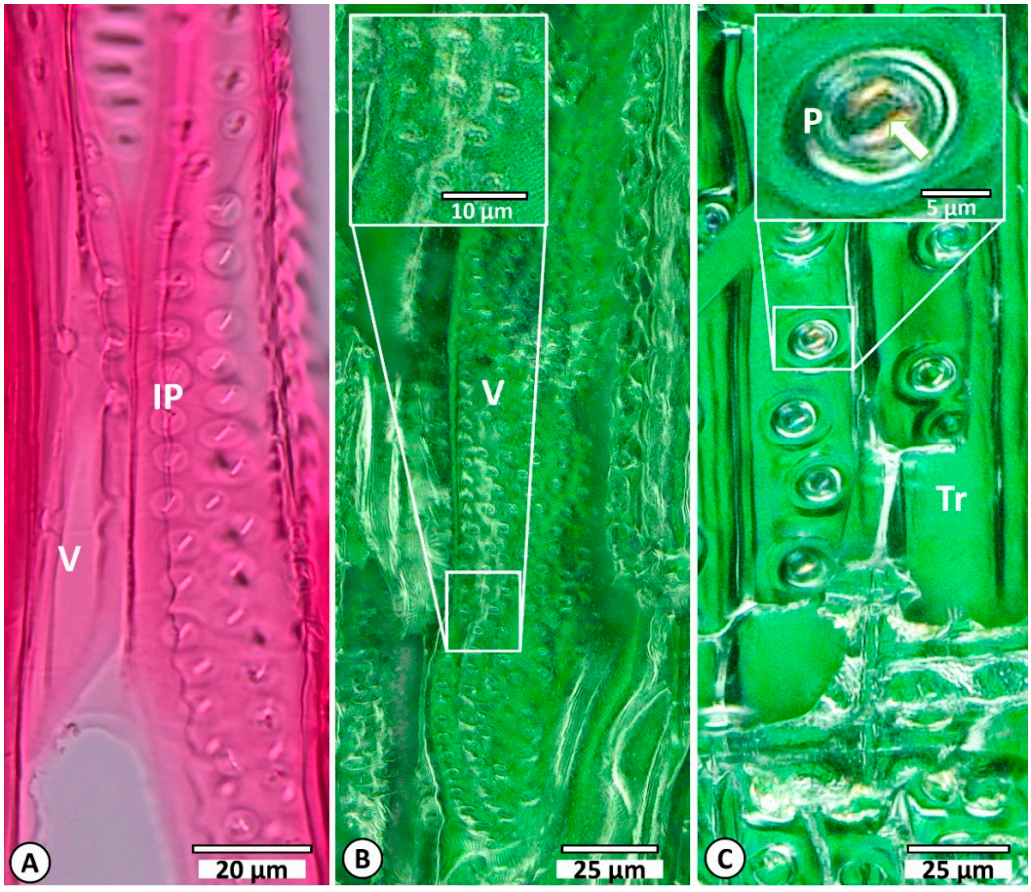

Figure 9. Three-dimensional-reflected light microscopy of (**A**) *Fagus sylvatica*: tangential section with vessels (V) and intervessel pits (IP); (**B**) *F. sylvatica*: three-dimensional presentation (charcoal fragment/3D-RLM) of tangential section with vessels (V) and a blown-up section with individual pits

that are fused with the surrounding tissue; (**C**) *Pinus sylvestris*: three-dimensional presentation (charcoal fragment/3D-RLM) of radial section with early wood tracheids (Tr) and blown-up section with a single pit (P) of which the pit pore cannot be clearly differentiated from the surrounding tissue (arrow).

As can be seen from Figure 9B, there was no opportunity to determine pit size in charred beech as is possible in virgin beech (Figure 9A). Pits and the adjacent tissues have fused together and become deformed during the charring process. The phenomenon of fused tissue is well known in the literature [12,15,29,30].

The same problem was recognised when determining the pit aperture sizes of the pine pits. Again, the individual tissue structures within the pits were no longer to be clearly distinguishable from one another (Figure 9C). As the change in pit aperture height ultimately corresponds to the same axis as the vertical pit height, the measurement of the pit aperture height was also discarded for this reason but pit height was analysed.

As can be seen in Figure 10A,B, the macroscopic structures of the wood are completely preserved. The vessels and rays in beech and the tracheids in pine show no damage or deformation. For example, the axial resin ducts in pine are still clearly visible. The deformation of the individual epithelial cells of the intercellular canals is only visible at high resolution. However, this may have occurred during processing, as the surfaces must first be broken for the 3D reflective light microscopy scans. The structural change therefore can be interpreted as a uniform volume change (shrinkage) in the sense of extreme drying. Major structural changes only occurred in pits that fused with adjacent tissue. Structural elements such as vessel and tracheid extensions were measured in a tangential direction, those of pit openings in an axial direction. The results are given in Table 6.

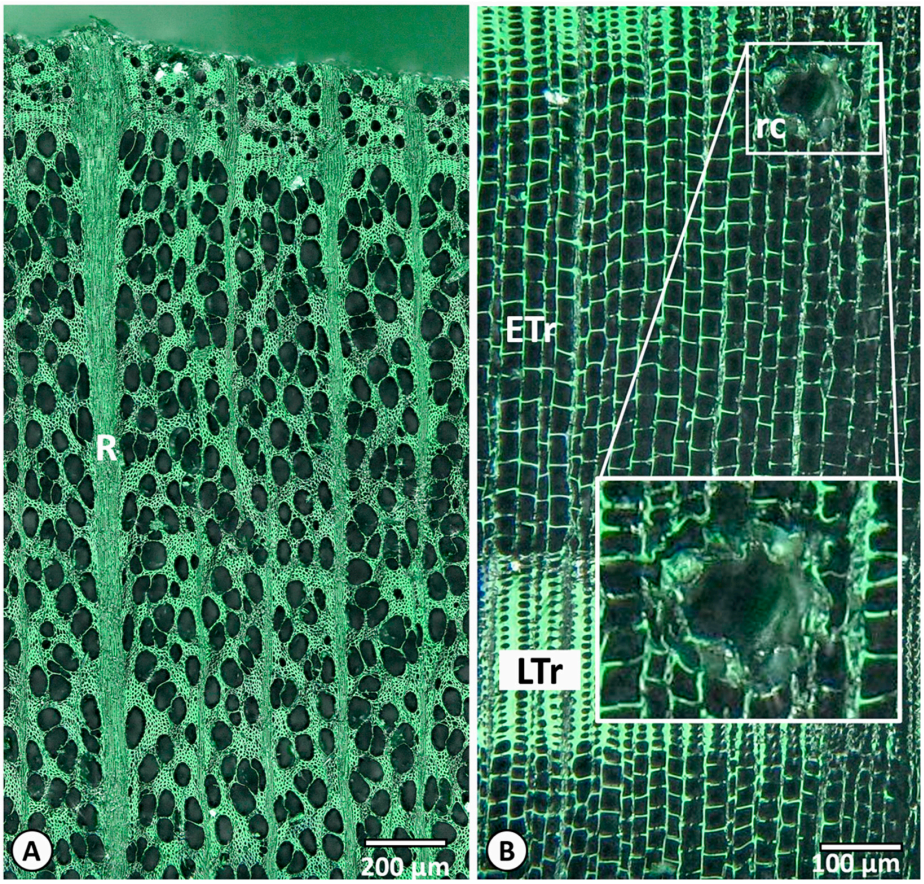

Figure 10. Three-dimensional-reflected light microscopy of (**A**) *Fagus sylvatica*: three-dimensional presentation (charcoal fragment/3D-RLM) of the transverse section with rays (R); (**B**) *Pinus sylvestris*:

three-dimensional presentation (charcoal fragment/3D-RLM) of transverse section with early wood tracheids (ETr) and late wood tracheids (LTr) and blown-up section with axial intercellular resin canal (rc).

The mean value of three beech wood vessels was 76.3 ± 10.5 µm. The charred samples shrank by about 35% to 49.8 ± 9.7 µm in the tangential direction. Pine wood tracheids showed mean values of 34.7 ± 7.5 µm and pine BC of 22.4 ± 4.4 µm, corresponding to a shrinkage of about 35.5%. Both types of wood behaved almost identically, with shrinkage in the tangential direction. In the axial direction, the pit diameter shrank by about 23% from 22.3 ± 2.2 µm in wood to 17.2 ± 1.7 µm in BC.

It is known from solid wood that shrinkage is not isotropic. From the swollen state, when saturated with water, beech/pine wood shrinks on average about 11.8/7.7% in the tangential direction, about 5.8/4.0% in the radial direction and about 0.3/0.4% in the axial direction when bone dry [20]. These figures must be taken into account when comparing cell dimensions. Wood samples were analysed at room temperature and ambient relative humidity, corresponding to wood moisture of approximately 12%. The samples in Figure 8 represent a swollen state of wood due to sample preparation for microscopy.

Identical cubes of beech (BC1) and pine (PC1) from Pyr_{red} were analysed first by microscopy and then by mercury porosimetry to compare the pore results of the two methods. In contrast to porosimetry, which covers all types of pores, the IAWA microscopic evaluation only looks at some specific cell structures in a specific way (see Section 2). Diameters from microscopy and porosimetry slightly differ. The mean diameter of larger pine BC pores is below 20 µm by porosimetry and about 25 µm by microscopy. Larger beech BC pores are about 30 µm in porosimetry and 53 µm in microscopy.

Regarding wood structure and the structure of BC with its fine pores, especially the pores of pine BC with tangential tracheid diameters of about 22 µm and inter tracheid connections with pit diameters of about 17 µm and pit aperture diameters two to three times smaller than the pit diameters, the question arises whether microorganisms such as archaea and bacteria are able to penetrate the charcoal pores in AD. Figure 11 shows typical sizes of archaea and bacteria [31] compared to charcoal pores (Figure 7). Most microrganisms have an elongated shape and some are three-dimensional. The lower values in Figure 11 correspond to the "diameters" of individual cells and the upper values to their longitudinal extent.

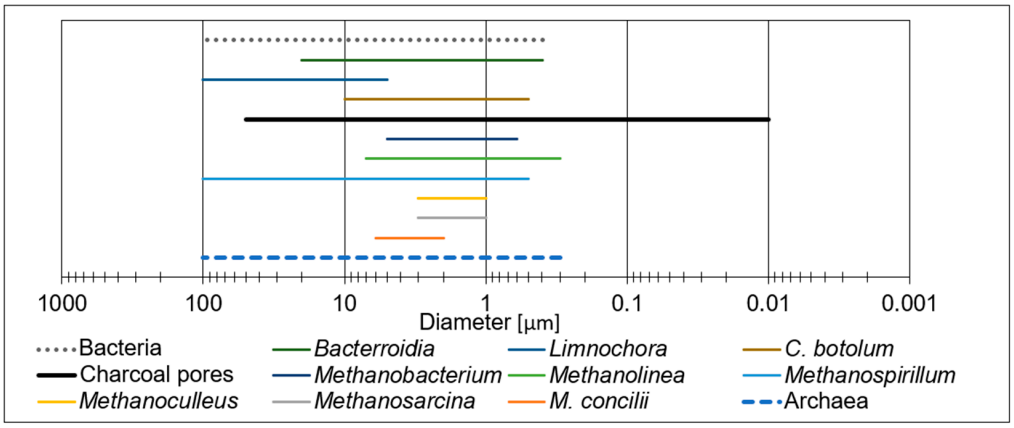

Figure 11. Sizes of selected archaea, bacteria and charcoal pores.

According to Figure 11, by size, individual microorganisms have a chance of penetrating the charcoal pores. However, microorganisms often live together in communities bound together by biofilm. To check whether microorganisms had penetrated the BC cubes during AD incubation, we opened the cubes, extracted material and analysed it using fluorescence microscopy.

Staining of the biochar cubes with red-fluorescing nucleic acid stain PI coupled to the green-fluorescing nucleic acid stain SYTO9 showed the presence of microorganisms inside the biochar cubes. As is typical for LIVE/DEAD staining, viable microorganisms showed strong green fluorescence and weak ones red fluorescence. The ratio of fluorescent dyes used for LIVE/DEAD staining was 1:1. As can be seen in Figure 12, the microorganisms agglomerated within the biochar material, indicating that biochar provides a habitat for microbial consortia.

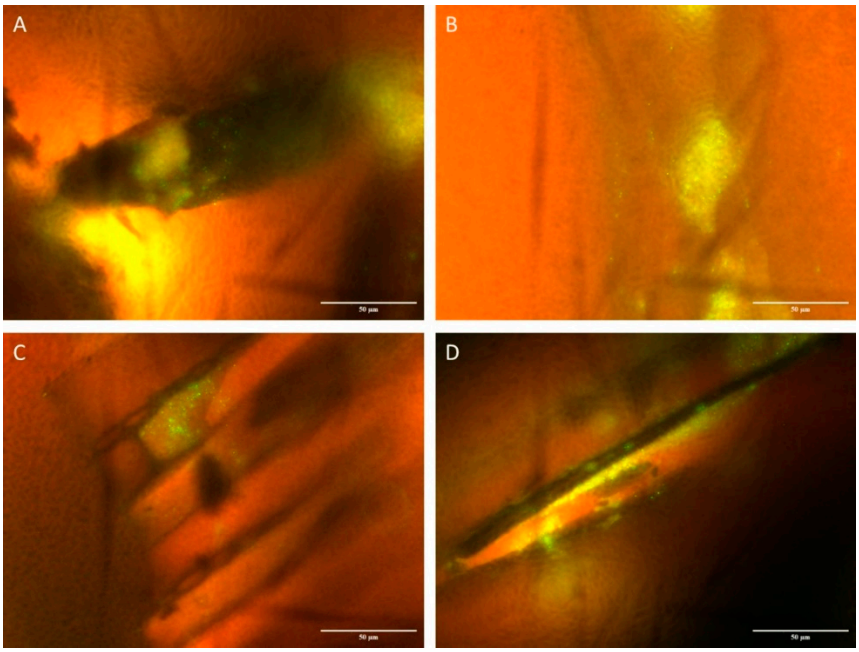

Figure 12. Fluorescence microscopy images of the presence of microorganisms in biochar cubes incubated in AD ((**A**,**B**) are BC cubes from Pyr_{red}, (**C**,**D**) from Pyr_{ox}).

Anticipating the individual results of AD with BC (details will be published elsewhere), we found that the addition of BC can increase the gas yield in inhibited systems, whereby we can demonstrate differences between BC from beech and BC from pine and the influence of particle size.

4. Conclusions

BC cubes made of beech and pine, charred under identical conditions, hardly differ in their chemical composition. Structurally, however, the difference is striking, as beech has relatively few large vascular pores in addition to dense fibrous and parenchymal tissue with very small pores, while pine shows a very even network of tracheid pores of about the same size.

Mercury (Hg) porosimetry is considered by Brewer C. E. et al. [26] to be a suitable method for pore characterisation of biochar, at least pore sizes in the area >1 µm. However, 3D-reflected light microscopy is more realistic and shows larger pore diameters than Hg-porosimetry.

Although the structure of beech and pine wood and the charcoal made from them give reasons for doubt, regarding colonisation inside BC cubes of approximate size $6 \times 6 \times 6\,mm^3$, microorganisms have been detected inside the cubes by fluorescence microscopy.

The structure of BC in terms of pore structure given by the wood source and particle size is the most important characteristic for its influence on AD.

Author Contributions: Conceptualisation, H.K., J.S. and R.F.; funding acquisition, H.K., J.S. and R.F.; investigation, H.K., J.S., P.G.P. and V.H.; methodology, H.K., J.S., T.S. and V.H.; project administration, J.S. and R.F.; resources, H.K., J.S., R.F. and V.H.; visualisation, H.K., P.G.P. and V.H.; writing—original

draft, H.K. and V.H.; writing—review and editing, H.K. and R.F. All authors have read and agreed to the published version of the manuscript.

Funding: This research was funded by Fachagentur für Nachwachsende Rohstoffe e.V., grant number 2220WD007.

Data Availability Statement: The original contributions presented in the study are included in the article, further inquiries can be directed to the corresponding author/s.

Conflicts of Interest: The authors declare no conflicts of interest. The funders had no role in the design of the study; in the collection, analyses, or interpretation of data; in the writing of the manuscript; or in the decision to publish the results.

References

1. Nelles, M.; Angelova, E.; Deprie, K.; Kornatz, P.; Rensberg, N.; Schaller, S.; Selig, M. Stand und Perspektiven der energetischen Verwertung von Biomasse in Deutschland (Translation: Status and perspectives of energy recovery from biomass in Germany). *Rostock. Bioenergy Forum.* **2023**, *114*, 13–36.
2. DESTATIS Statistisches Bundesamt. *Land- und Forstwirtschaft, Fischerei—Wirtschaftsdünger Tierischer Herkunft in Landwirtschaftlichen Betrieben/Landwirtschaftszählung. (Translation: Agriculture, Forestry and Fisheries—Manure of Animal Origin on Agricultural Holdings/Agricultural census)*; DESTATIS: Wiesbaden, Germany, 2021; S. 142, Fachserie 3 Reihe 2.2.2.
3. Mlinar, S.; Weig, A.R.; Freitag, R. Influence of NH3 and NH4+ on anaerobic digestion and microbial population structure at increasing total ammonia nitrogen concentrations. *Bioresour. Technol.* **2022**, *361*, 127638. [CrossRef] [PubMed]
4. Kumar, S.; Jain, M.; Chhonkar, P. A note on stimulation of biogas production from cattle dung by addition of charcoal. *Biol. Wastes* **1987**, *20*, 209–215. [CrossRef]
5. Mumme, J.; Srocke, F.; Heeg, K.; Werner, M. Use of biochars in anaerobic digestion. *Bioresour. Technol.* **2014**, *164*, 189–197. [CrossRef] [PubMed]
6. Kumar, M.; Dutta, S.; You, S.; Luo, G.; Zhang, S.; Show, P.L.; Sawarkar, A.D.; Singh, L.; Tsang, D.C. A critical review on biochar for enhancing biogas production from anaerobic digestion of food waste and sludge. *J. Clean. Prod.* **2021**, *205*, 127–143. [CrossRef]
7. Tang, S.; Wang, Z.; Liu, Z.; Zhang, Y.; Si, B. The Role of Biochar to Enhance Anaerobic Digestion: A Review. *J. Renew. Mater.* **2020**, *8*, 1033–1052. [CrossRef]
8. Heitkamp, K.; Latorre-Pérez, A.; Nefigmann, S.; Gimeno-Valero, H.; Vilanova, C.; Jahmad, E.; Abendroth, C. Monitoring of seven industrial anaerobic digesters supplied with biochar. *Biotechnol. Biofuels* **2021**, *14*, 14. [CrossRef] [PubMed]
9. Lü, F.; Luo, C.; Shao, L.; He, P. Biochar alleviates combined stress of ammonium and acids by firstly enriching Methanosaeta and then Methanosarcina. *Water Res.* **2016**, *90*, 34–43. [CrossRef] [PubMed]
10. Rudi, W. Mikroskopischer Bau des Holzkörpers. (Translation: Microscopic Structure of the Wood Structure). In *Anatomie des Holzes*; VEB Fachbuchverlag: Leipzig, Germany, 1998.
11. Harald, C.; Coté, A.; Wilfred, A.; Arnold, C.D. Microscopic Structure of Wood. In *Wood Structure and Identification*, 2nd ed.; Syracuse University Press: Syracuse, NY, USA, 1979.
12. Haag, V.; Dremel, K.; Zabler, S. Volumetric imaging by micro computed tomography: A suitable tool for wood identification of charcoal. *IAWA J.* **2022**, *44*, 210–224. [CrossRef]
13. Korte, H.; Al-Saadi, A.J.A.; Nelles, M.; Sprafke, J. Holzkohleherstellung in einem 90-Liter-Reaktor: Ein Erfahrungsbericht (Translation: Charcoal production in a 90-liter reactor: A field report). *Rostock. Bioenergieforum* **2023**, *114*, 173–178.
14. EBC-European Biochar Certification. Analytical Methods. 20 September 2023. Available online: https://www.european-biochar.org/en/ct/8-Analytical-Methods (accessed on 13 June 2023).
15. Zemke, V.; Haag, V.; Koch, G. Wood identification of charcoal with 3D-reflected light microscopy. *IAWA J.* **2020**, *41*, 478–489. [CrossRef]
16. Hapla, F.; Saborowski, J. Stichprobenplanung für Holzanatomische Untersuchungen (Translation: Sample Design for Wood Anatomical Examinations). *Holz Als Roh-Und Werkstoff.* **1987**, *45*, 141–144. [CrossRef]
17. International Organization for Standardization. *Evaluation of Pore Size Distribution and Porosity of Solid Materials by Mercury Porosimetry and Gas Adsorption*; ISO: Geneva, Switzerland, 2016; pp. 1–19. Available online: https://www.iso.org/standard/56005.html (accessed on 1 July 2024).
18. Deutsches Institut für Normung. *Determination of Solid State Density*; Deutsches Institut für Normung [din]: Washington, DC, USA, 2019. Available online: https://standards.globalspec.com/std/257178/din-66137-1 (accessed on 1 July 2024).
19. Deutsches Institut für Normung. *Determination of the Specific Surface Area of Solids by Gas Adsorption-BET Method (ISO 9277:2010)*; Deutsches Institut für Normung [din]: Washington, DC, USA, 2014. Available online: https://webstore.ansi.org/standards/din/diniso92772014?srsltid=AfmBOor6WiQv1RWuIXN2pLMh8x3QjXLhno4yBV0UBDrj-ypxfWl9QR-t (accessed on 1 July 2024).
20. Fengel, D.; Wegener, G. *Wood—Chemistry, Ultrastructure, Reactions*; Walter de Gruyter: Berlin, Germany; New York, NY, USA, 1984.
21. Zhang, C.; Zhang, Z.; Zhang, L.; Li, Q.; Li, C.; Chen, G.; Zhang, S.; Liu, Q.; Hu, X. Evolution of the functionalities and structures of biochar in pyrolysis of poplar in a wide temperature range. *Bioresour. Technol.* **2020**, *304*, 123002. [CrossRef]

22. Reza, S.; Afroze, S.; Bakar, M.S.; Saidur, R.; Aslfattahi, N.; Taweekun, J.; Azad, A.K. Biochar characterization of invasive Pennisetum purpureum grass: Effect of pyrolysis temperature. *Biochar* **2020**, *2*, 239–251. [CrossRef]
23. Yang, H.; Yan, R.; Chen, H.; Lee, D.H.; Zheng, C. Characteristics of hemicellulose, cellulose and lignin pyrolysis. *Fuel* **2007**, *86*, 1781–1788. [CrossRef]
24. Popescu, C.-M.; Popescu, M.-C.; Singurel, G.; Vasile, C.; Argyropoulos, D.S.; Willfor, S. Spectral Characterization of Eucalyptus Wood. *Appl. Spectrosc.* **2007**, *61*, 1168–1177. [CrossRef] [PubMed]
25. Chen, Y.; Yang, H.; Wang, X.; Zhang, S.; Chen, H. Biomass-based pyrolytic polygeneration system on cotton stalk pyrolysis: Influence of temperature. *Bioresour. Technol.* **2012**, *107*, 411–418. [CrossRef] [PubMed]
26. Brewer, C.E.; Chuang, V.J.; Masiello, C.A.; Gonnermann, H.; Gao, X.; Dugan, B.; Driver, L.E.; Panzacchi, P.; Zygourakis, K.; Davies, C.A. New approaches to measuring biochar density and porosity. *Biomass. Bioenergy* **2014**, *66*, 176–185. [CrossRef]
27. Richter, H.G.; Grosser, D.; Heinz, I.; Gasson, P.E. Iawa List of Microscopic Features for Softwood Identification. *IAWA J.* **2004**, *25*, 1–70. [CrossRef]
28. Richter, H.G.; Dallwitz, M.J. Commercial Timbers: Descriptions, Illustrations, Identification, and Information Retrieval. In English, French, German, Portuguese and Spanish. 2000 Onwards, Version 2019. Available online: http://delta-intkey.com (accessed on 27 March 2024).
29. Haag, V.; Koch, G.; Kaschuro, S. Womit grillen wir da eigentlich? Wissenschaftliche Untersuchungen zeigen, dass viele Chargen zumindest fehlerhaft deklariert sind. (Translation: What are ae actually barbecuing with? Scientific studies show that many batches are at least incorrectly declared). *Holz Zentralblatt* **2017**, *143*, 876.
30. Balzano, A.; Cufar, K.; Krže, L.; Merela, M. *Wood Identification of Charcoal with Confocal Laser Scanning Microscopy: Identifikacija lesa Oglja s Pomočjo Konfokalne Laserske Vrstične Mikroskopije*; Les/Wood: Liptovský Mikuláš, Slovakia, 2020; Volume 69, pp. 21–35.
31. Whitman, W.B. *Bergey's Manual of Systematics of Archaea and Bacteria*; Bergey's Manual Trust: Athens, GA, USA, 2015.